JOURNAL OF CATALYSIS **165,** 33–44 (1997)
ARTICLE NO. CA971447

The Kinetics of Ammonia Synthesis over Ru-Based Catalysts

1. The Dissociative Chemisorption and Associative Desorption of N_2

O. Hinrichsen, F. Rosowski, A. Hornung, M. Muhler,* and G. Ertl

Fritz-Haber-Institut der Max-Planck-Gesellschaft, Faradayweg 4-6, D-14195 Berlin, Germany

Received April 10, 1996; revised August 13, 1996; accepted August 20, 1996

The dissociative chemisorption of N_2 is generally accepted to be the rate-determining step of ammonia synthesis over Ru-based catalysts. The interaction of N_2 with the following three Ru catalysts has been studied: Ru supported on Al_2O_3 (Ru/Al_2O_3) and on MgO (Ru/MgO), and Ru/MgO promoted with cesium (Cs–Ru/MgO). Temperature-programmed N_2 adsorption and desorption experiments and the isotopic exchange reaction $^{14}N^{14}N + {}^{15}N^{15}N \rightleftharpoons 2\,{}^{14}N^{15}N$ were performed in a microreactor flow system. A microkinetic analysis based on the Langmuir–Hinshelwood Hougen–Watson mechanism has been applied to these kinetic experiments yielding the rate constants of dissociative chemisorption (k_{ads}) and associative desorption (k_{des}). The dissociation of N_2 was indeed found to be a slow and activated process. Ru/Al_2O_3 was found to be rather inactive for N_2 dissociation. Ru/MgO turned out to be a heterogeneous system with respect to the interaction with N_2 due to the presence of promoted active sites which dominate the rate of N_2 dissociation. Promotion by cesium was observed to enhance both k_{ads} and k_{des} significantly and rendered the Ru metal surfaces uniform toward the interaction with N_2. The initial sticking coefficient and the rate of desorption of N_2 derived from the microkinetic models are in good agreement with results obtained with Ru single crystal surfaces under ultra-high vacuum conditions.

1. INTRODUCTION

Over the past two decades, extensive research has been carried out to develop a new catalyst generation for ammonia synthesis. Aika and co-workers have studied numerous Ru-based catalyst systems to elucidate the role of the support and of the alkali promoter (1). The authors consider Cs-promoted Ru catalysts supported on MgO (Cs–Ru/MgO) to be one of the second-generation catalysts for large-scale NH_3 synthesis (1). Tennison and co-workers at British Petroleum developed Cs- and Ba-copromoted Ru supported on carbon into an alternative to the commercially used Fe catalysts prepared from fused magnetite (2). In 1992, the retrofitted 600 ton NH_3/day Ocelot plant started to produce NH_3 using promoted Ru catalysts supported on carbon based on the Kellogg Advanced Ammonia Process (KAAP) (3, 4). The Ru-based catalysts permit milder operating conditions compared with the magnetite-based systems, such as low synthesis pressure (70–105 bars compared with 150–300 bars) and lower synthesis temperatures, while maintaining higher conversion than a conventional system (5).

In our laboratory, a systematic study of the interaction of N_2, H_2, and NH_3 with polycrystalline Ru catalysts and with Ru single crystal surfaces has been performed aiming at a detailed understanding of the elementary steps of NH_3 synthesis. In analogy to NH_3 synthesis on Fe, the rate-determining step for Ru-based catalysts is generally accepted to be the dissociative chemisorption of N_2. A detailed understanding of the interaction of N_2 with Ru catalysts thus provides the key for establishing consistent microkinetic models for NH_3 synthesis.

We recently presented a detailed kinetic study of the associative desorption of N_2 from Ru supported on MgO (Ru/MgO) (6). The rate of dissociative chemisorption (r_{ads}) of N_2 on Ru/MgO was derived by varying the N_2 exposure conditions. The determination of the resulting coverage of adsorbed atomic nitrogen (N-$*$) was based on the integration of the subsequently obtained N_2 TPD peaks yielding the kinetic adsorption parameters $A_{ads} = 2 \times 10^{-6}(\mathrm{Pa \cdot s})^{-1}$ and $E_{ads} = 27$ kJ/mol (6). The extrapolated sticking coefficient of about 10^{-13} at 300 K is in agreement with the inertness of Ru(0001) in UHV towards dissociative chemisorption of N_2. However, if the whole catalytic surface were in this state, then the resulting rate of N_2 dissociation would be several orders of magnitude lower than the observed rate of NH_3 formation. Hence it was concluded that only a small fraction of the total Ru metal surface area of Ru/MgO seemed to be highly active, dominating the rate of NH_3 formation. Such promoted sites might originate from a strong interaction with the alkaline earth support at the interface.

On the close-packed Ru(0001) single crystal surface, the dissociation of N_2 has been found to be a slow and activated process (7, 8). Recently, an initial N_2 sticking

* To whom all correspondence should be addressed.

0021-9517/97 $25.00

coefficient as low as $(1 \pm 0.8) \times 10^{-12}$ was measured on Ru(0001), Ru(10$\bar{1}$0) and Ru(11$\bar{2}$1) surfaces at room temperature which was found to be independent of surface morphology (9). On Ru(0001) even the maximum exposure of 0.15 mbar N_2 for 1000 min did not result in a higher coverage of N-$*$ than 2% of the monolayer coverage $\Theta_N^{max} = 0.25$ (9), indicating a further decrease of the sticking coefficient with increasing coverage of N-$*$. Tsai and Weinberg (10) performed a detailed analysis of their experimental results for N_2 desorption following NH_3 decomposition. They arrived at $E_{des} = 184$ kJ/mol for the activation energy of desorption with an associated preexponential factor of $A_{des} = 2 \times 10^{12}\ s^{-1}$. These values have been confirmed by Shi *et al.* (11) who obtained saturation with N-$*$ by using the hot filament of an ionization gauge to activate N_2.

The determination of ultra-low sticking coefficients makes great demands on the purity of the gas to be adsorbed, the residual gas present in the setup, and the cleanness of the adsorbent. Other examples of recent determinations of ultra-low sticking coefficients are the dissociative chemisorption of CH_4 on the Ni(100) single crystal plane ($s_0 = 1.7 \times 10^{-9}$ at 400 K, $E_A = 59 \pm 1.5$ kJ/mol) by Nielsen *et al.* (12) and the dissociative chemisorption of CO_2 on Cu(100) ($s_0 = 7.5 \times 10^{-12}$ at 500 K, $E_A = 93 \pm 5$ kJ/mol) by Rasmussen *et al.* (13).

On Ru single crystal surfaces, molecular N_2 was found to exist either as a physisorbed species at 40 K (14) or bound end-on in a weakly chemisorbed state (γ-N_2-$*$) in the temperature range 70–120 K (15–18). Contrary to Fe, there is no indication for the participation of a di-σ bound chemisorbed molecular precursor labeled α-N_2-$*$ for N_2 dissociation on Ru single crystal surfaces (19). The dissociation step is therefore written in one equation in which $*$ denotes a free active site on the surface,

$$N_2 + 2* \rightleftharpoons 2\ N\text{-}* \qquad [1]$$

On polycrystalline Ru samples, IR measurements revealed the influence of the alkali promoter on the stretching frequency of N_2-$*$ which was interpreted in the frame of a charge transfer mechanism (1). The observed shifts of the N_2 IR absorption band to lower wavenumbers were 421 cm^{-1} for Cs–Ru/MgO, 163 cm^{-1} for Ru/MgO, 117 cm^{-1} for Ru/Al_2O_3 and 111 cm^{-1} for Ru/SiO_2 compared with the gas phase stretching frequency. The higher shifts for Cs–Ru/MgO and Ru/MgO were assigned to an electron donation by the alkali promoter and the basic MgO support, respectively (1, 20).

The present first part of the series focuses on the interaction of N_2 with supported Ru catalysts, i.e., Ru/Al_2O_3, Ru/MgO, and Cs–Ru/MgO. The preparation of the catalysts from high-purity $Ru_3(CO)_{12}$, and γ-Al_2O_3, and MgO was found to result in long-term and high-temperature stable NH_3 synthesis catalysts (21). Temperature-programmed N_2 adsorption (TPA) and desorption (TPD) experiments and the isotopic exchange reaction (IER) $^{14}N^{14}N + {}^{15}N^{15}N \rightleftharpoons 2\,{}^{14}N^{15}N$ were performed in a microreactor flow system equipped with a calibrated mass-spectrometer. These experiments have in common that their kinetics are determined by both the rate of dissociative chemisorption and the rate of associative desorption. Readsorption of N_2 within the porous catalyst grains packed in a fixed bed may occur during the TPD experiment, and the dissociative chemisorption of N_2 is followed by the associative desorption of N_2 at higher temperatures during the TPA experiment.

A microkinetic analysis based on the Langmuir–Hinshelwood Hougen–Watson (LHHW) mechanism has been applied to the kinetic experiments with N_2 yielding a consistent set of rate constants of dissociative chemisorption (k_{ads}) and of associative desorption (k_{des}). For Cs–Ru/MgO, the values of k_{ads} and k_{des} derived from the TPD and IER experiments allowed us to predict the outcome of the TPA experiment with respect to both peak positions and shapes. The initial sticking coefficients and the rates of desorption of N_2 derived from the microkinetic models are in good agreement with results obtained with Ru single crystal surfaces. Thus microkinetics served successfully as a tool to bridge the gap between Ru single crystals in UHV and supported Ru catalysts operating at high pressure.

The second part of the series deals with the microkinetics of NH_3 synthesis based on the LHHW mechanism using the three supported catalysts mentioned above. It is demonstrated that the rate constants derived in the present study can successfully be integrated in microkinetic models consisting of all the elementary steps of NH_3 synthesis. Additional information is obtained from H_2 TPD experiments and from the temperature-programmed surface reaction (TPSR) $N\text{-}* + 1.5\,H_2 \rightarrow NH_3 + *$. The microkinetic models are able to fit the rate of NH_3 synthesis over a wide range of experimental conditions. The third part presents a combination of transient and steady-state kinetic experiments which help to unravel the mechanism of NH_3 dissociation over Ru-based catalysts.

2. EXPERIMENTAL

Ru/Al_2O_3, Ru/MgO, and Cs–Ru/MgO were prepared by impregnation of high purity γ-Al_2O_3 (99.99%, Johnson Matthey) and MgO (Johnson Matthey, Puratronic, 99.996% metals basis), respectively, with a solution of $Ru_3(CO)_{12}$ (Johnson Matthey) in THF following the procedures in references (22–24). Details about the preparation of the catalysts are given in Ref. (21). The Ru loading obtained was approximately 5 wt%. For the Cs–Ru/MgO catalyst, Ru/MgO was further impregnated with a solution of $CsNO_3$ (Strem, 99.99%) in H_2O/acetone to obtain an atomic ratio

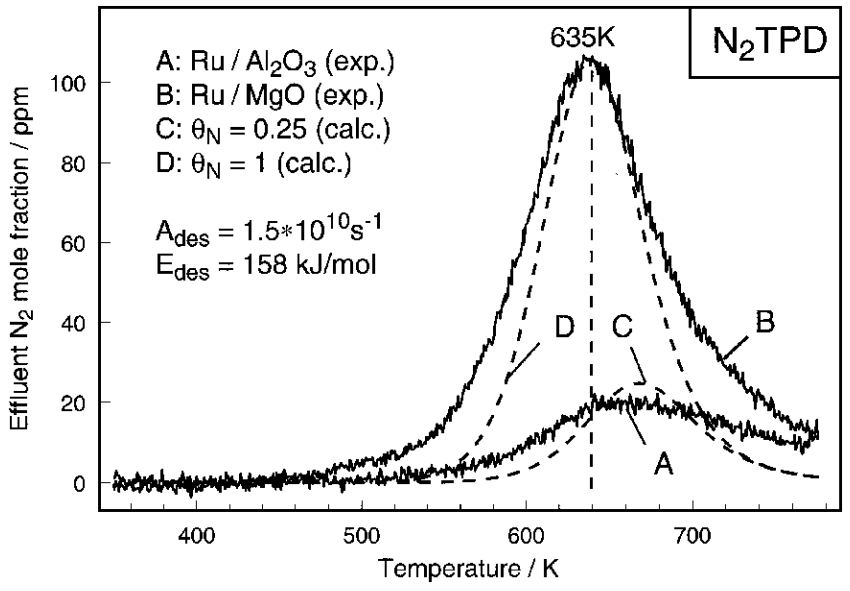

FIG. 1. Experimental N_2 TPD data (solid lines) for Ru/Al_2O_3 (trace A) and Ru/MgO (trace B). The TPD data were obtained by dosing N_2 at 573 K for 14 h and subsequent cooling in N_2 to room temperature. The heating rate was 5 K/min in both experiments. Traces C and D (dashed lines) are the modeling results using $k_{des} = 1.5 \times 10^{10}\ s^{-1} \cdot \exp(-158\ kJ/mol/RT)$ with initial condition $\Theta_N = 0.25$ for Ru/Al_2O_3 (trace C) and $\Theta_N = 1.0$ for Ru/MgO (trace D).

of Cs/Ru = 1 : 1. The reduction was carried out in synthesis gas ($N_2/H_2 = 1/3$) using a flow of 80 Nml/min and a heating ramp of 30 K/h up to 773 K (673 K for Cs–Ru/MgO). The catalyst weight was 1 g using the sieve fraction of 0.25–0.8 mm except for the N_2 TPD experiments with Ru/Al_2O_3 and Ru/MgO shown in Fig. 1 in which 0.2 g of catalyst were used. Additional experiments were performed to ensure that the catalytic reactions were limited by the surface chemical kinetics. Mass and heat transport limitations were found to be absent. Further details are given in Ref. (25).

The Ru metal area was determined by volumetric H_2 chemisorption in the quartz U-tube of an Autosorb 1-C setup (Quantachrome) following the procedure described in Ref. (26). Details of the characterization by XPS, XRD, and TEM are given in Ref. (21). All kinetic experiments were conducted in a high-pressure stainless steel flow apparatus equipped with a calibrated quadrupole mass spectrometer described in detail in Ref. (27). The setup has been extended by a gas mixing unit (base pressure $<10^{-8}$ mbar) which was pressurized up to 10 bar with the gases used for the IER and TPA experiments. The gases were supplied by Linde and had the following purities: He, 99.9999%; N_2, 99.9999%; H_2, 99.9999%; and the mixture of 25% N_2 in H_2 used as synthesis feed gas, 99.9996%. He, N_2, and H_2 were additionally passed through a cold trap at 178 K. The feed gas was further purified by means of a self-designed guard reactor (28). For the IER experiments, the isotope $^{15}N_2$ supplied by Isotec was used which contained 0.3% residual $^{14}N_2$.

Prior to carrying out a TPD, IER, or TPA experiment, NH_3 synthesis was run at a steady state at 773 K (673 K for Cs–Ru/MgO). Then the gas composition was changed from the stoichiometric synthesis gas mixture to 50 Nml/min He at the same temperature followed by flushing with He for 120 min. In order to obtain a saturated coverage of N-* prior to a N_2 TPD experiment, a flow of 50 Nml/min N_2 was used. Subsequently, the catalyst was cooled down to room temperature and the flow was switched to 50 Nml/min He before the temperature ramp was started (6). For the IER and TPA experiments, the catalysts were cooled in He. The IER was monitored by flowing roughly equimolar mixtures of about 1.2–1.5% $^{14}N_2$ and $^{15}N_2$ in He through the catalyst bed while covering the temperature range from 300 to 773 K (673 K for Cs–Ru/MgO). Following the experimental procedure described by Fastrup (29), the TPA experiments were carried out with 50 Nml/min of a dilute mixture of N_2 (6600 and 6900 ppm, respectively) in He. A linear heating ramp of 5 K/min and 10 K/min, respectively, was applied in the temperature range from 160 to 773 K (673 K for Cs–Ru/MgO). The TPA experiment required accurately linear temperature ramps and a highly stable and sensitive mass spectrometer (Balzers GAM 445).

3. MODELING

In the microkinetic analysis of the IER, the microreactor was modeled as a series combination of well-mixed reactors in order to simulate the plug flow reactor (PFR) behavior. A system of nonlinear equations was solved which consisted of the steady-state equations for all surface intermediates, the site balance on the catalyst, and the material balances for the gaseous species. In the fitting routine, generalized

regression software (GREG) developed by Stewart *et al.* (30) was used to optimize the activation energies and the preexponential factors of k_{ads} and k_{des}.

The transient TPD and TPA experiments were modeled by a continuous stirred tank reactor (CSTR). The resulting set of ordinary differential equations was solved using a variable-order, variable-step method implementing the backward differentiation formula method found in the library of NAG (31). Modeling the reactor as a PFR changed the ordinary differential equations to partial differential equations. The set of partial differential equations was solved using a collocation method which is also found in the library of NAG (31). A negligible reactor effect on the analysis of the TPA and TPD experiments was found, thus justifying the assumption of CSTR behavior.

4. RESULTS

In the following sections, the results of the metal area determination and of the catalytic activity measurements obtained with Ru/Al_2O_3, Ru/MgO, and Cs-Ru/MgO are presented first. Subsequently, the TPD and the IER results are presented followed finally by the TPA results.

Ru Metal Area Determination and Catalytic Activity

The H_2 chemisorption results are summarized in Table 1. Based on a stoichiometry of Ru/H = 1/1, 236, 260, and 138 μmol Ru surface atoms per gram catalyst were derived for Ru/Al_2O_3, Ru/MgO, and Cs–Ru/MgO, respectively. Both TEM and XRD measurements confirmed an increase in particle size from about 2 nm for Ru/MgO to 3–10 nm for Cs–Ru/MgO due to the aqueous impregnation with $CsNO_3$ (21).

In order to achieve saturation with N-$*$, Ru/Al_2O_3 and Ru/MgO were exposed to a flow of 50 Nml/min N_2 at 573 K for 14 h and then cooled down in N_2 to room temperature. The results of subsequently performed TPD experiments are shown in Fig. 1. The integration of the N_2 TPD trace of the Ru/MgO catalyst (trace B in Fig. 1) yielded 28.2 μmol/g N_2. By varying the temperature and the length of the N_2 exposure, Rosowski *et al.* (6) were able to show that the value of 56.4 μmol N-$*$/g actually corresponded to the saturation coverage of N-$*$. Based on 260 μmol Ru surface atoms/g obtained with H_2 chemisorption, this amount of N-$*$ corresponds to a coverage of $\Theta_N = 0.22$ in good agreement with the saturation coverage of $\Theta_N^{max} = 0.25$ observed on Ru(0001) (9).

TABLE 1

Results of the H_2 and N_2 Chemisorption Measurements after NH_3 Synthesis Based on H/Ru = 1/1 and N/$*$ = 1/1. NH_3 Synthesis Was Run at 773 K with Ru/MgO and Ru/Al_2O_3, and at 673 K with Cs–Ru/MgO

	Ru/Al_2O_3	Ru/MgO	Cs–Ru/MgO
H_2 monolayer capacity/μmol/g	118	130	69
Ru surface atoms/μmol/g	236	260	138
N_2 monolayer capacity/μmol/g	28.2	28.2	12.2
Active sites S/μmol/g	56.4	56.4	24.5

TABLE 2

Catalytic Activity of the Ru/Al_2O_3, Ru/MgO, and Cs–Ru/MgO Catalysts at 588 K Determined after Several Weeks on Stream under the Following Conditions: $p = 1$ bar, $Q = 120$ Nml/min, $N_2:H_2 = 1:3$, $w_{cat} = 0.138$ g. The turnover frequency r^{TOF} has been calculated according to $r^{TOF} = (x_{NH_3} \cdot Q)/(22414\ \text{Nml/mol} \cdot w_{cat} \cdot S)$

	Ru/Al_2O_3	Ru/MgO	Cs–Ru/MgO
x_{NH_3}(ppm)	38	300	616
r (μmol/(s · g))	$2.47 \cdot 10^{-2}$	0.19	0.40
r^{TOF} (s^{-1})	$4.4 \cdot 10^{-4}$	$3.5 \cdot 10^{-3}$	$1.6 \cdot 10^{-2}$

However, it was not possible to achieve saturation with N-$*$ on Ru/Al_2O_3 even when dosing N_2 at pressures up to 10 bar. Contrary to Ru/MgO, the integration of the N_2 TPD peak of Ru/Al_2O_3 (trace A in Fig. 1) obtained after the same N_2 exposure as for Ru/MgO yielded only 7 μmol/g N_2 equivalent to 14 μmol N-$*$/g. It has to be pointed out that about the same H_2 uptake was observed for both catalysts. On Cs–Ru/MgO, saturation with N-$*$ was achieved by cooling in a flow of 50 Nml/min N_2 from 673 K to room temperature within about 3 h yielding 24.5 μmol N-$*$/g. These N_2 adsorption experiments point to the following sequence with respect to r_{ads}: Cs–Ru/MgO > Ru/MgO $\gg$ Ru/Al_2O_3.

The number of active sites on metal catalysts is usually assumed to be equal to the total number of surface atoms determined by, e.g., H_2 chemisorption. The difficulties encountered in this field are discussed in a recent review (32). Since the present microkinetic modeling is intended to describe the dissociative chemisorption of N_2 forming N-$*$ and the associative desorption of N-$*$, it appears to be more reasonable to set the number of active sites equal to the saturation amount of N-$*$. Thus problems associated with H_2 chemisorption like spill-over from the metal to the support and ill-defined adsorption stoichiometries are avoided (33). Since H_2 chemisorption revealed about the same uptake of H_2 for Ru/Al_2O_3 and Ru/MgO, 56.4 μmol/g active sites were assumed for Ru/Al_2O_3 in the following.

Based on the saturation coverages of N-$*$ shown in Table 1, the turnover frequencies of ammonia synthesis r^{TOF} were calculated from the rates specified in Table 2 which were measured after several weeks under synthesis conditions. The catalytic activity of Cs–Ru/MgO decreased somewhat initially, whereas no significant deactivation was observed for the unpromoted catalysts. The catalytic activity closely reflects the trend observed for r_{ads}: Cs–Ru/MgO > Ru/MgO > Ru/Al_2O_3. The ratio of the r^{TOF} values

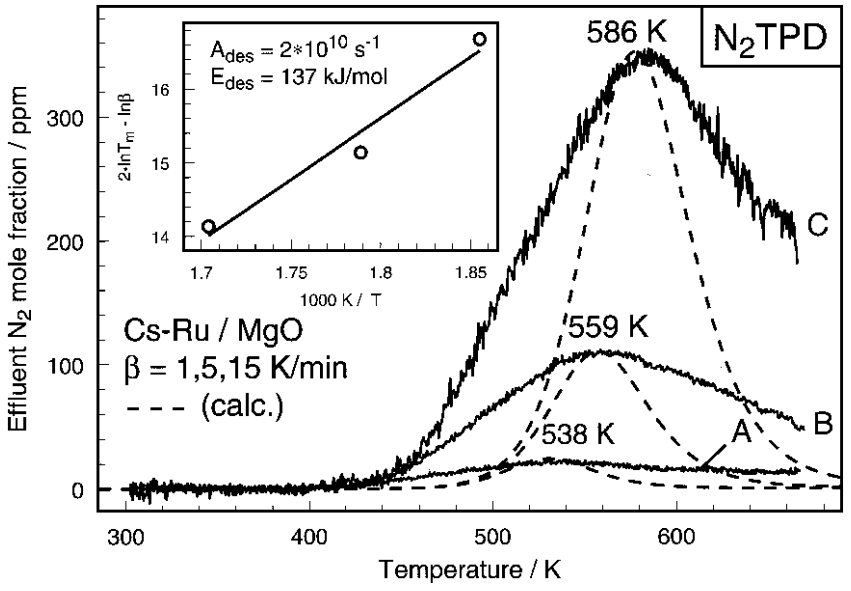

FIG. 2. Experimental N_2 TPD data (solid lines) for Cs–Ru/MgO. The TPD data were obtained by cooling in a flow of 50 Nml/min N_2 from 673 to 298 K. The heating rates were 1 (trace A), 5 (trace B), and 15 (trace C) K/min. The inset displays the microkinetic analysis of the activation energy and the frequency factor for associative desorption without readsorption using linear regression resulting in $k_{des} = 2.0 \times 10^{10}\ s^{-1} \cdot \exp(-137\ kJ/mol/RT)$. The modeled TPD traces using k_{des} are shown as dashed lines and were scaled in height.

determined at 588 K with Cs–Ru/MgO and Ru/Al_2O_3 using a constant feed gas flow was found to be about 40. Nwalor and Goodwin (34) derived a ratio of about 100 at roughly constant conversion for $K–Ru/SiO_2$ and Ru/SiO_2 at 673 K. These ratios illustrate that the presence of the alkali promoter is essential for Ru-based catalysts used for NH_3 synthesis.

Temperature-Programmed Desorption of N_2

Based on a detailed microkinetic analysis, Rosowski *et al.* (6) derived a preexponential factor $A_{des} = 1.5 \times 10^{10}$ molecules/site · s and an activation energy $E_{des} = 158 \pm 4$ kJ/mol for the associative desorption of N_2 from Ru/MgO. The dashed TPD traces in Fig. 1 were calculated without readsorption for Ru/MgO and Ru/Al_2O_3 with these kinetic parameters. The initial relative coverages of N-∗ were assumed to be $\Theta_N = 1.0$ in the case of Ru/MgO and $\Theta_N = 0.25$ for Ru/Al_2O_3. The initial coverage of 0.25 for Ru/Al_2O_3 is based on the ratio of 14 μmol N-∗/g obtained by integrating trace 1 in Fig. 1 with 56.4 μmol N-∗/g as the assumed saturation value. The good agreement between experimental and calculated TPD peak positions and shapes justifies this assumption, indicating that the desorption kinetics of N_2 from Ru/MgO and Ru/Al_2O_3 are rather similar. Furthermore, the full widths at half maximum (FWHM) differ by only 22 K for Ru/MgO, indicating the absence of readsorption of desorbed N_2 molecules within the catalyst bed. Readsorption would give rise to asymmetric TPD peak broadening to higher temperatures due to the delayed elution of the desorbed N_2 molecules. The good agreement of the FWHMs also demonstrates that the desorption parameters are essentially independent of coverage in agreement with a coverage-dependent analysis of N_2 TPD data obtained with the Ru(0001) single crystal surface (10).

The N_2 TPD data for Cs–Ru/MgO obtained with various heating rates are shown in Fig. 2. By heating at 1 (trace A), 5 (trace B), and 15 (trace C) K/min in He, broad and rather symmetric N_2 TPD peaks centered at about 538, 558, and 586 K, respectively, were obtained. The integration of the traces with 5 and 15 K/min is not straightforward, since the mole fraction of N_2 has not yet reached the baseline at the end temperature of 673 K. Hence the temperature-programmed surface reaction (TPSR) N-∗ + 3/2H_2 → NH_3 + ∗ (35) performed by flowing H_2 over preadsorbed N-∗ was used additionally to confirm the value of 24.5 μmol N-∗/g for Cs–Ru/MgO specified in Table 1.

The symmetric TPD peak shapes observed for Cs–Ru/MgO (Fig. 2) also indicate the absence of readsorption at higher temperatures. Plotting $\ln(T_{max}^2/\beta)$ versus $1/T_{max}$ as shown in the inset of Fig. 2 yields $A_{des} = 1.5 \pm 0.5 \times 10^{10}$ molecules/site · s and $E_{des} = 137 \pm 4$ kJ/mol by applying linear regression assuming associative desorption. Modeling the TPD results obtained with Cs–Ru/MgO with the kinetic parameters without readsorption yields the dashed traces in Fig. 2 which were normalized to the same height as the corresponding experimental trace. The experimental and calculated FWHMs differ by about 70 K, indicating the presence of repulsive adsorbate–adsorbate interaction at high Θ_N. It is noteworthy that the onset of N_2 desorption is as low as about 420 K. The rate constants of desorption are summarized in Table 3.

TABLE 3

Rate Constants $k_i = A_i \cdot \exp(-E_i/RT)$ for $N_2 + 2* \rightleftharpoons 2\,N\text{-}*$ Derived from the TPD, IER, and TPA Experiments

	A_{ads} $(kPa \cdot s)^{-1}$	E_{ads} (kJ/mol)	Technique	A_{des} (s^{-1})	E_{des} (kJ/mol)	Technique
Ru/Al_2O_3	56	60.6	IER	$1.5 \cdot 10^{10}$	158.0	TPD, IER
Ru/MgO	56	48.0	IER	$1.5 \cdot 10^{10}$	158.0	TPD
	56	40.0	TPA (Fig. 5, B)	$2.0 \cdot 10^{10}$	137.0	TPA (Fig. 5, B), IER
	56	60.6	TPA (Fig. 5, C)	$1.5 \cdot 10^{10}$	158.0	TPA (Fig. 5, C)
	56	$48.0 + 40 \cdot \Theta_N$	TPA	$1.5 \cdot 10^{10}$	158.0	TPA
Cs–Ru/MgO	56	33.0	IER, TPA	$2.0 \cdot 10^{10}$	137.0	TPD, IER, TPA

In a recent publication, Rosowski *et al.* (6) concluded that a certain fraction of the total Ru metal surface area of Ru/MgO seemed to have a significantly higher activity dominating the rate of NH_3 formation. A small additional TPD peak at about 500–550 K was observed when dosing N_2 at temperatures up to 473 K at atmospheric pressure which seemed to saturate faster at lower dosing temperatures compared with the main TPD peak at 635 K. Hence the N_2 TPD experiment with Ru/MgO was repeated using 1.0 g of catalyst instead of 0.2 g (trace B in Fig. 1) to enhance the TPD peak heights. A dilute mixture of 6900 ppm N_2 in He was dosed at 373 K for 30 min using a flow of 50 Nml/min. This low exposure was chosen to selectively populate the active sites with a higher r_{ads}. The resulting TPD data shown in Fig. 3 clearly reveal the presence of two TPD peaks at about 540 K and 670 K. Based on the overall adsorption kinetics previously derived neglecting the nonuniformity of the Ru metal surfaces (6), a coverage of $\Theta_N = 10^{-3}$ is predicted. The achieved relative coverage of $\Theta_N = 0.11$ is significantly higher, confirming the suggested existence of active sites with a higher r_{ads}.

The identification of the additional sites with higher r_{ads} and r_{des} is assisted by microkinetic analysis. The inset in Fig. 3 shows two calculated TPD traces using k_{des} (Table 3) derived for Ru/MgO (trace B) and for Cs–Ru/MgO (trace C) with $\Theta_N = 1$ to illustrate the temperature range of desorption for unpromoted and promoted active sites. The calculated traces were scaled in height to the experimental trace to facilitate the comparison. The good agreement in peak positions suggests that the N_2 TPD peak at lower temperatures is due to desorption from promoted sites which may originate from the interaction with the MgO support.

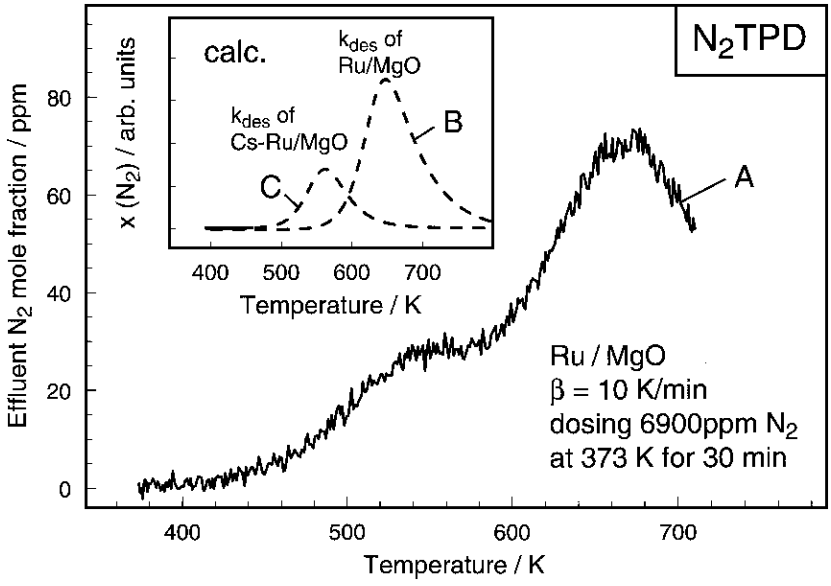

FIG. 3. Experimental N_2 TPD data for Ru/MgO (trace A, solid line) were obtained subsequent to dosing a dilute mixture of 6900 ppm N_2 in He at 373 K for 30 min. The heating rate was 10 K/min. The inset shows the modeling results (dashed lines) assuming two independent sites. The rate constants used were those derived for Ru/MgO (trace B) and for Cs–Ru/MgO (trace C) listed in Table 3. The TPD peaks were calculated assuming $\Theta_N = 1$ and were scaled in height to trace A.

Hence these highly active sites are labeled promoted active sites in the following.

Isotopic Exchange Reaction

The dissociation kinetics of N_2 were studied in more detail by exposing the catalysts to a dilute mixture of $^{14}N_2$ and $^{15}N_2$ in He using a total flow of 50 Nml/min. The rate of formation of $^{14}N^{15}N$ was monitored at steady state as a function of temperature:

$$^{14}N^{14}N + {}^{15}N^{15}N \rightleftharpoons 2\,{}^{14}N^{15}N. \qquad [2]$$

The effluent mole fractions of $^{14}N^{15}N$ are shown as solid traces A, B, and C in Fig. 4 for Ru/Al_2O_3, Ru/MgO, and Cs–Ru/MgO, respectively. At temperatures below 400 K, $^{14}N_2$ and $^{15}N_2$ dissociate, giving rise to a saturated coverage of ^{14}N-$*$ and ^{15}N-$*$, but the product $^{14}N^{15}N$ cannot be formed due to the too high E_{des} in this temperature range. Hence the onset of the $^{14}N^{15}N$ formation is governed by r_{des} as observed for Cs–Ru/MgO at about 440 K in agreement with the TPD onset (Fig. 2). It is remarkable that for Ru/MgO about the same onset temperature was found, indicating the presence of some obviously promoted active sites with a higher r_{ads} than the majority of active sites.

The results shown in Fig. 4 clearly reflect the differences in the rates of N_2 dissociation for the three catalysts. Cs–Ru/MgO has the highest r_{ads} followed by Ru/MgO. At a temperature of about 620 K the mole fraction of $^{14}N^{15}N$ was observed to bend over for Cs–Ru/MgO (solid trace C in Fig. 4) reaching a final value of 0.58% $^{14}N^{15}N$ at a temperature of 673 K. Taking the mole fractions of 0.34% $^{14}N_2$ and 0.28% $^{15}N_2$ at 673 K into account, the value of the equilibrium constant defined as

$$K = \frac{\left[{}^{14}N^{15}N\right]^2}{[{}^{14}N_2]\cdot[{}^{15}N_2]} \qquad [3]$$

is equal to 3.5 close to the value of 4 in case of complete isotopic randomization. For Ru/MgO (trace B), the equilibrium mole fractions of 0.64%, 0.35%, and 0.30% for $^{14}N^{15}N$, $^{14}N_2$, and $^{15}N_2$, respectively, were reached at 740 K, yielding $K = 3.9$. It was not possible to reach equilibrium using Ru/Al_2O_3 (trace A in Fig. 4) even at 773 K due to its low r_{ads} which did not allow either to achieve saturation with N-$*$ when dosing with 1 bar N_2 for 14 h at 573 K.

The kinetics of the IER experiment are determined by k_{ads} and k_{des}. Since the latter were already derived from the TPD experiments, the microkinetic analysis of the IER experiments allows us to obtain k_{ads}. Without knowing k_{des} in advance, the temperature range of the IER experiments is too narrow to allow an unequivocal determination of both rate constants due to the compensation of preexponential factors and activation energies.

The IER experiment with Ru/Al_2O_3 was modeled using k_{des} derived for Ru/MgO (traces C and D in Fig. 1). The agreement obtained is rather poor, using $k_{ads} = 56\ (\mathrm{kPa\cdot s})^{-1} \exp(-60.6\ \mathrm{kJ/mol/RT})$. At higher temperatures, the kinetic model overestimates the experimental results, indicating a coverage-dependent decrease of k_{ads}. Furthermore, the microkinetic modeling assumes Θ_N to be close to unity at lower temperatures, in clear contradiction to the experimental results since it was not possible to achieve a

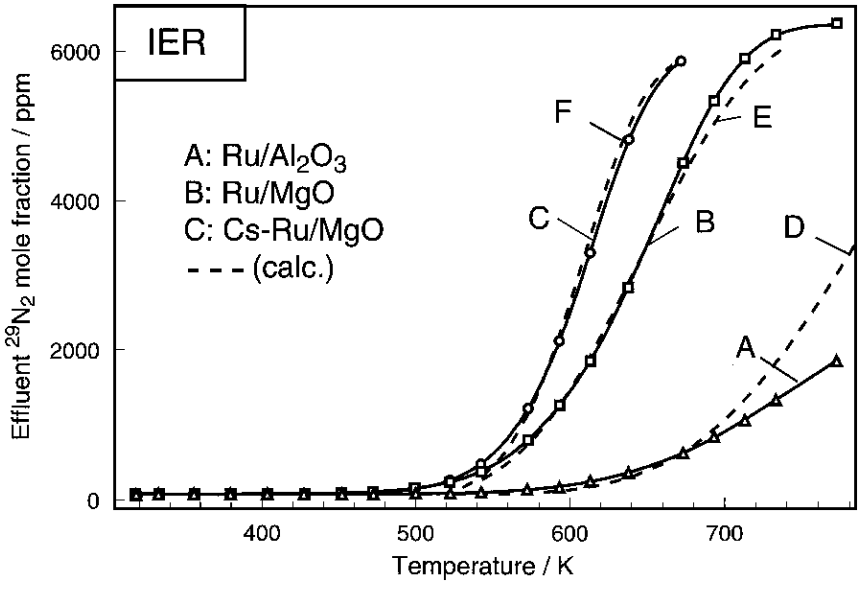

FIG. 4. Experimental IER data (solid lines) for Ru/Al_2O_3 (trace A), Ru/MgO (trace B), and Cs–Ru/MgO (trace C) using a total flow of 50 Nml/min of 0.61% $^{14}N_2$ and 0.97% $^{15}N_2$, 0.67% $^{14}N_2$ and 0.60% $^{15}N_2$, and 0.64% $^{14}N_2$ and 0.59% $^{15}N_2$ in He, respectively. The traces D, E, and F displayed as dashed lines result from the microkinetic modeling using the kinetic parameters summarized in Table 3.

higher relative coverage of N-∗ than $\Theta_N = 0.25$. Hence both rate constants in Table 3 for Ru/Al_2O_3 should be considered only as estimates for the initial rate constants.

For Ru/MgO, good agreement between the experimental and the calculated IER traces was obtained (traces B and E in Fig. 4, respectively). The IER experiment was modeled using $A_{ads} = 56\ (kPa \cdot s)^{-1}$ and $E_{ads} = 48$ kJ/mol based on 56.4 μmol/g active sites. For the desorption parameters, the kinetic parameters of Cs–Ru/MgO were chosen because of the same onset temperature of the formation of $^{14}N^{15}N$ observed for both catalysts. The IER experiment is obviously dominated by a small amount of promoted active sites with higher r_{ads} and r_{des}. Comparing the IER activities of Ru/MgO and Ru/Al_2O_3 clearly shows that unpromoted sites are almost inert toward dissociative chemisorption of N_2.

The modeling of the steady-state IER rate of Cs–Ru/MgO yields $A_{ads} = 56\ (kPa \cdot s)^{-1}$ and $E_{ads} = 33$ kJ/mol using the desorption parameters for Cs–Ru/MgO derived from the N_2 TPD experiments shown in Fig. 2. The calculated trace F in Fig. 4 is in good agreement with the experimental result (trace C in Fig. 4). It is remarkable that for both Cs–Ru/MgO and Ru/MgO it was possible to achieve such good agreement based on LHHW kinetics without coverage-dependent rate constants.

Temperature-Programmed Adsorption of N_2

Finally, the N_2 adsorption kinetics were investigated by performing the N_2 TPA experiment. By flowing a dilute mixture of N_2 in He through the catalyst bed while increasing the temperature linearly from 160 K on, it is possible to monitor on-line the adsorption of N_2 at lower temperatures corresponding to a decrease of the N_2 mole fraction and the desorption of N_2 at higher temperatures corresponding to an increase in the N_2 mole fraction. The traces shown in the following are net mole fractions of N_2, i.e., negative mole fractions indicate adsorption and positive mole fractions indicate desorption.

Within the experimental detection limit of about 20 ppm, it was not possible to detect TPA peaks for Ru/Al_2O_3 as expected from the inertness of this catalyst toward N_2 dissociation. The rate constant of adsorption estimated from the IER modeling would predict a TPA peak at 634 K with a height of 314 ppm and a FWHM of 84 K using 6900 ppm N_2 in He and a heating rate of 10 K/min. This was clearly not the case, indicating again that k_{ads} of Ru/Al_2O_3 specified in Table 3 should only be considered as an initial rate constant which decreases even more with increasing Θ_N.

The additional N_2 TPD peak at lower temperatures shown in Fig. 3 and the low IER onset temperature of the Ru/MgO catalyst have been interpreted as evidence for promoted sites with desorption kinetics similar to those of the Cs-promoted sites on Cs–Ru/MgO. Figure 5 shows the experimental TPA result for Ru/MgO (trace A) and the modeling results (dashed traces). Two adsorption peaks were observed, indicating indeed that two different active sites are present. The first adsorption peak is located at about 480 K followed by a deeper adsorption peak at 570 K. The total amount adsorbed was 6.5 μmol/g N_2 equivalent

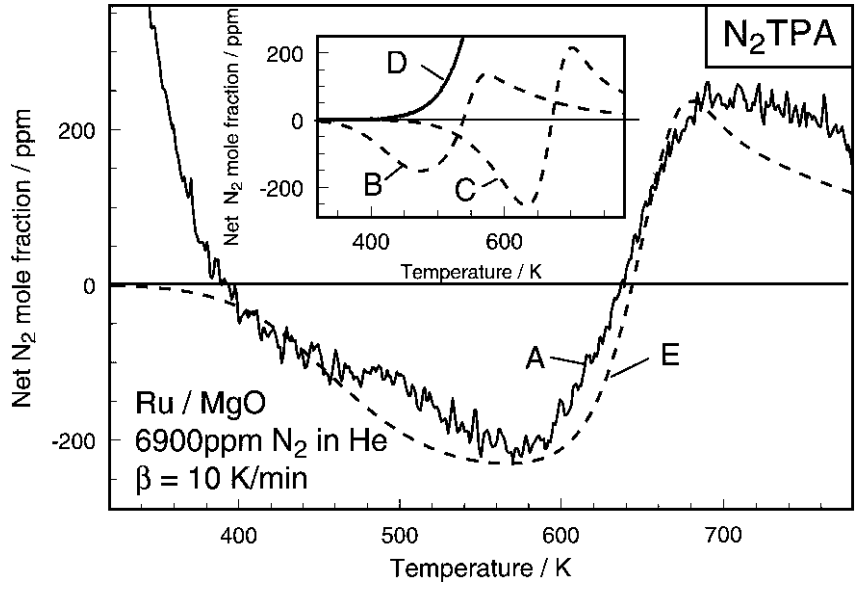

FIG. 5. N_2 TPA data for Ru/MgO: Comparison of the experimental data (trace A) as solid line and the modeling results (traces B, C, E) as dashed lines is shown. The TPA experiment was performed with a dilute mixture of 6900 ppm N_2 in He using a total flow of 50 Nml/min and a heating rate of 10 K/min. The inset shows the modeling results assuming two independent sites (traces B and C) using the kinetic parameters summarized in Table 3. Trace D is the mole fraction of $^{14}N^{15}N$ formed during the IER experiment with Ru/MgO already shown as trace B in Fig. 4. The result of the modeling using $E_{ads} = (48.0 + 40 \cdot \Theta_N)$ kJ/mol is shown as trace E.

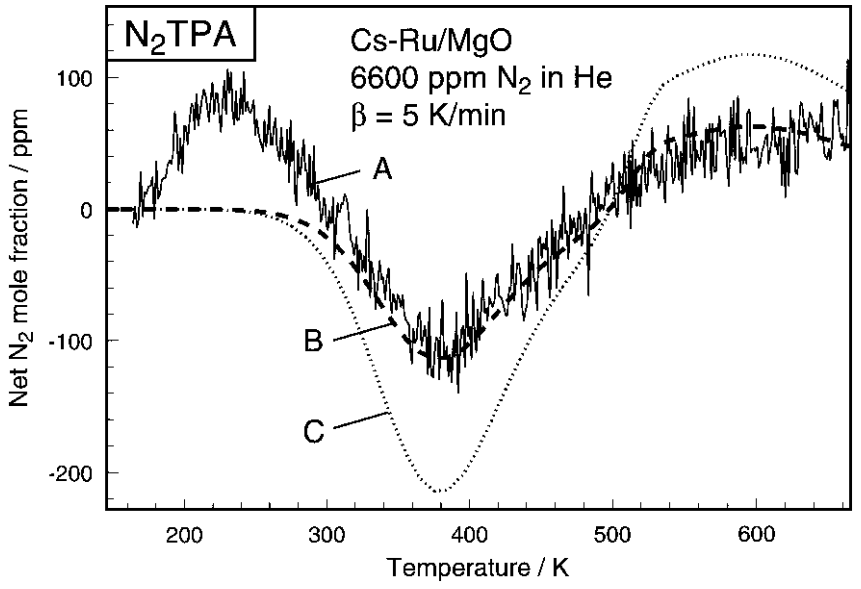

FIG. 6. N_2 TPA data for Cs−Ru/MgO: Comparison of the experimental data (trace A) and the modeling results obtained with 13 μmol/g (trace B) and 24.5 μmol/g active sites (trace C) is shown. The TPA experiment was performed with a dilute mixture of 6600 ppm N_2 in He using a total flow of 50 Nml/min and a heating rate of 5 K/min.

to 13 μmol/g active sites. Assuming two different kinds of active sites, the highest fractional coverage defined as the number of adsorbed species divided by the total number of sites of all types is estimated to be about 0.2 for the promoted sites on which adsorption occurs at lower temperatures.

The inset of Fig. 5 shows the TPA modeling results for the Ru/MgO catalyst based on a LHHW mechanism assuming two independent sites on the surface (trace B, promoted sites, and trace C, unpromoted sites) without diffusion from one site to the other. The two TPA traces are in good agreement with the experimental result (trace A in Fig. 5). The rate constants of dissociative adsorption and associative desorption obtained for the two active sites are summarized in Table 3. The rate constants of the unpromoted sites were taken from the modeling of the IER using Ru/Al_2O_3. Since r_{des} from promoted sites is significantly higher than r_{des} from unpromoted sites, the modeling of the TPA experiment predicts the onset of desorption significantly below the experimentally observed onset temperature of 630 K. This is illustrated by trace D in the inset of Fig. 5 which is the mole fraction of $^{14}N^{15}N$ formed during the IER experiment with Ru/MgO already shown as trace B in Fig. 4.

Alternatively, in order to work with as simple a model as possible, the overall kinetics of the N_2 TPA experiment for Ru/MgO can be described by using a coverage-dependent rate constant of adsorption based on the rate constants of Ru/MgO in Table 3, assuming 56.4 μmol/g active sites. The modeling result is shown as a trace E in Fig. 5. In the calculation, the activation energy of adsorption was modeled to vary linearly with coverage: $E_{ads} = 48\ \text{kJ/mol} + w \cdot \Theta_N$, with $w = 40$ kJ/mol. This simple approach implies that the heat of adsorption decreases linearly with coverage as required by thermodynamic consistency.

Using r_{ads} and r_{des} derived for Cs−Ru/MgO from the IER and TPD experiments (Table 3), it was possible to predict the TPA trace B shown in Fig. 6 which is in good agreement with the experimental result (trace A). At lower temperatures, a fairly symmetric adsorption peak with a minimum at about 380 K is observed. At about 450 K, the desorption of N_2 sets in, giving rise to a broad desorption peak maximum at about 580 K. Both the shape and the position of the adsorption and desorption peaks are closely reproduced by the values of k_{ads} and k_{des}, respectively, listed in Table 3.

However, for the modeling of the TPA experiment only 13 μmol/g active sites had to be used. As shown by trace C in Fig. 6 calculated with 24.5 μmol/g, the shape of the TPA trace scales linearly with the total amount of active sites. Modeling the TPA experiment with 24.5 μmol/g active sites and different kinetic parameters would lead to completely different peak shapes and peak positions. The microkinetic analysis therefore suggests that indeed only 13 μmol/g active sites are present under the low temperature conditions of the TPA experiment. It has to be noted that the saturated amount of 24.5 μmol N-$*$/g was obtained by cooling in N_2 from 673 K to room temperature.

The TPA experiments with Ru/MgO and Cs−Ru/MgO both displayed the desorption of N_2 below room temperature. This observation might serve as an indication for the desorption of the molecular α-N_2-$*$ precursor delayed by readsorption in the catalyst bed. However, the identification of species desorbing at low temperatures in

a flow system is not without pitfalls as demonstrated in Ref. (36). The delayed elution of e.g. γ-N_2 out of micropores might be another explanation of this phenomenon. Further studies are in progress to elucidate the role of the molecular precursor for dissociative chemisorption (37).

5. DISCUSSION

The discussion focuses on the role of cesium and on microkinetic analysis as a tool to bridge the gap between studies under UHV conditions and at high presssure.

By modeling N_2 sorption experiments under UHV conditions using the kinetic parameters listed in Table 3, the relationship between supported Ru catalysts and Ru single crystal surfaces is investigated in the following. Using a heating rate of 10 K/s, the kinetic associative desorption parameters $A_{\mathrm{des}} = 1.5 \times 10^{10}\,\mathrm{s}^{-1}$ and $E_{\mathrm{des}} = 158\,\mathrm{kJ/mol}$ derived from the TPD experiments with Ru/MgO and Ru/Al_2O_3 result in a TPD peak at about 750 K in good agreement with N_2 TPD experiments with the Ru(0001) single crystal surface (10, 11). Obviously, the supported Ru crystallites offer similar adsorption sites for atomic nitrogen like planar Ru single crystal surfaces on which N-$*$ was found to occupy threefold hollow sites (38). It seems reasonable to assume that locally the same adsorption geometry should be available on supported Ru crystallites. The good agreement between the experimental and the calculated FWHM of the N_2 TPD peak therefore indicates that predominantly Ru(0001) facets are exposed to the gas phase. Kim *et al.* (39) investigated the photoemission from xenon adsorbed on polycrystalline Ru powder concluding that 70% of the surface consisted of Ru(0001) facets.

The kinetic adsorption parameters $A_{\mathrm{ads}} = 56\ (\mathrm{kPa \cdot s})^{-1}$ and $E_{\mathrm{ads}} = 60.6\,\mathrm{kJ/mol}$ derived for Ru/Al_2O_3 from the IER experiments yield a sticking coefficient at room temperature of 10^{-15} compared with $(1 \pm 0.8) \times 10^{-12}$ derived for Ru single crystal surfaces (9). The data reported by Dietrich *et al.* (9) provide some evidence that the sticking coefficient may decrease even further with increasing Θ_{N} since 4×10^{-13} was obtained for $\Theta_{\mathrm{N}} = 0.12$ as the highest relative coverage obtained on Ru(1010). It has to be pointed out that both with Ru single crystal surfaces and with unpromoted Ru/Al_2O_3, it was experimentally not feasible to achieve saturation with N-$*$ by dosing N_2. For Cs–Ru/MgO, the values of $E_{\mathrm{ads}} = 33\,\mathrm{kJ/mol}$ and of $E_{\mathrm{des}} = 137\,\mathrm{kJ/mol}$ were found to be lower by 27.6 kJ/mol and 21 kJ/mol, respectively. Extrapolating k_{ads} derived for Cs–Ru/MgO to room temperature results in a sticking coefficient of 5×10^{-11} which is in agreement with the enhanced sticking coefficient observed for Cs-promoted Ru single crystals (40).

The N_2 TPD peak at lower temperatures observed for Ru/MgO has been assigned to desorption from promoted active sites. However, the N_2 TPD peaks obtained with Ru(1010), and Ru(11$\bar{2}$1) were found to be at lower temperatures than the ones obtained with Ru(0001) (9). Hence the TPD peak might be assigned to desorption from more open Ru facets which might exist on Ru metal particles supported on MgO, but not on Al_2O_3. This structural hypothesis can be rejected for the following two reasons: First, the single crystal investigations on Ru(0001), Ru(1010), and Ru(11$\bar{2}$1) did not provide any evidence for N_2 dissociation being a structure-sensitive reaction on Ru (9). Even if more open Ru facets were present on Ru/MgO compared to Ru/Al_2O_3, these facets should not be more active than the close-packed Ru(0001) surface. Second, by applying high-resolution TEM, Datye *et al.* (41) observed the shape of Ru crystallites supported on model SiO_2 and MgO surfaces to be similar, i.e., MgO was not found to induce a special morphology of the supported Ru crystallites.

On the other hand, under the highly reducing NH_3 synthesis conditions at temperatures up to 773 K, it seems likely that oxygen vacancies are formed at the interface between the Ru crystallites and the MgO support which can act as electronic promoters. It has to be noted that Aika *et al.* (24) found $Ba(NO_3)_2$ to be the most effective promoter precursor among the alkaline earth metals. The oxygen defect chemistry of MgO and its relevance for the oxidative coupling of methane has been reviewed recently by Voskresenskaya *et al.* (42). This electronic hypothesis is supported by the similarity between Cs–Ru/MgO and Ru/MgO with respect to the kinetic parameters derived from the TPD, IER, and TPA experiments. These experiments clearly showed that the presence of Cs leads to enhanced rates of adsorption and desorption in agreement with the principle of microscopic reversibility. According to the electronic hypothesis, the alkaline earth support acts in a way similar to the alkali promoter. Correspondingly, the efficiency of the Cs promotion should be determined by the amount of oxygen vacancies determined by the degree of reduction of the (Cs + O)-coadsorbate layer under the reducing NH_3 synthesis conditions. Further studies using photoelectron spectroscopy are in progress which support the electronic hypothesis (43).

Both for the modeling of TPD and the TPA experiments with Ru/MgO, two independent sites were assumed without taking diffusion of N-$*$ into account. Since Ru/Al_2O_3 showed an almost negligible activity for the dissociation of N_2, the formation of N-$*$ should occur dominantly at the promoted sites at the interface to the MgO support from which N-$*$ should diffuse onto the Ru metal particle, thus populating the unpromoted sites, too. When including a diffusion step into the microkinetic model, a barrier height for diffusion of more than 100 kJ/mol was found to be necessary to roughly reproduce the experimental TPA and TPD data. Such a barrier seems to be rather high since on Ru(0001) terraces a value of about 30 kJ/mol was derived from STM measurements (38). However, it is reasonable to assume that the activation energy of diffusion over

mono- and polyatomic steps is significantly higher. These steps have to be overcome on a three-dimensional Ru crystallite to saturate its surface facets. Additionally, the influence of the promoting alkaline earth support on the diffusion barrier has to be taken into account. On the other hand, the nonuniformity of Ru/MgO with respect to the interaction with N_2 may be modeled by coverage-dependent kinetic parameters for the sake of simplicity, as shown in case of the TPA experiment using $E_{ads} = 48.0$ kJ/mol + 40 kJ/mol $\cdot \Theta_N$.

For the modeling of the TPA peak at 380 K observed for Cs–Ru/MgO, it was necessary to reduce the amount of active sites from 24.5 μmol/g to 13 μmol/g. Recent STM experiments showed that a solid-fluid phase equilibrium exists for coadsorbed Cs and O on Ru(0001) (44). At 440 K, the $(\sqrt{7} \times \sqrt{7})$R19° layer with a Cs/O ratio of 1/2 was found to be completely transformed into the fluid state (44). Hence at higher temperatures corresponding to NH_3 synthesis conditions, a significantly higher amount of promoted active sites should be present on Cs–Ru/MgO due to the melting of the coadsorbate layer. Ion scattering spectroscopy data recently obtained with K–Ru/MgO and K–Ru/C revealed that the Ru metal particles are indeed covered by the potassium promoter (43). Another consequence of this fluid-like behavior is that the Ru metal surfaces should be uniformly promoted. Since the presence of the Cs promoter was found to enhance r_{ads} and consequently r^{TOF} by several orders of magnitude, it is plausible that the uniformly (Cs + O)-covered Ru metal surfaces turned out to be highly active and uniform with respect to the dissociation of N_2. The comparison of r^{TOF} for Cs–Ru/MgO, Ru/MgO, and Ru/Al_2O_3 leads to the conclusion that the presence of the alkali or alkaline earth promoter is essential for Ru-based catalysts used for NH_3 synthesis.

The dominance of highly active sites has been identified as the reason why the nonuniformity of catalytic surfaces can be disregarded for numerous reactions (45). Recently we set up a microkinetic model based on a LHHW mechanism for Cs–Ru/MgO incorporating k_{ads} and k_{des} listed in Table 3 obtained by the present combined microkinetic analysis of the transient TPD/TPA experiments and the steady-state IER experiments (46). This model is additionally able to predict the results of H_2 TPD and TPSR experiments and the steady-state formation of NH_3 over a broad range of experimental conditions.

6. CONCLUSIONS

1. For both NH_3 synthesis and the N_2 isotopic exchange reaction, Cs–Ru/MgO was found to be more active than Ru/MgO. Ru/Al_2O_3 showed hardly any activity for both reactions. Correspondingly, it was possible to achieve a saturated coverage with adsorbed atomic nitrogen on Ru/MgO and Cs–Ru/MgO, but not on Ru/Al_2O_3 with a maximum relative coverage of only $\Theta_N = 0.25$ after 14 h at 573 K in N_2 at atmospheric pressure.

2. The rate constant of N_2 desorption from Cs–Ru/MgO was derived from TPD experiments with different heating rates yielding $A_{des} = 2.0 \times 10^{10}$ s^{-1} and $E_{des} = 137$ kJ/mol. The kinetics of N_2 desorption from Ru/Al_2O_3 appeared to be similar to the kinetics of Ru/MgO with $A_{des} = 1.5 \times 10^{10}$ s^{-1} and $E_{des} = 158$ kJ/mol.

3. The microkinetic analysis of the isotopic exchange reaction including k_{des} derived from TPD experiments yielded k_{ads} for all three catalysts. Only an estimate of the initial adsorption rate constant of Ru/Al_2O_3 was obtained due to its low activity which did not allow us to achieve complete isotopic randomization even at 773 K. For Ru/MgO and Cs–Ru/MgO, good agreement between the experimental and the calculated results was achieved. Cs–Ru/MgO turned out to have a higher r_{ads} ($A_{ads} = 56$ (kPa $\cdot$ s)$^{-1}$, $E_{ads} =$ 33 kJ/mol) than Ru/MgO ($A_{ads} = 56$ (kPa $\cdot$ s)$^{-1}$, $E_{ads} = 48$ kJ/mol). The Cs promoter was thus found to enhance both r_{ads} and r_{des}.

4. Evidence for the coexistence of two types of active sites on Ru/MgO was obtained by means of the TPD, IER, and TPA experiments. Highly active sites on Ru/MgO were identified by a small additional TPD peak at lower temperatures, the same onset temperature of $^{14}N^{15}N$ formation as Cs–Ru/MgO, and the observation of two TPA peaks. The identification of these sites as promoted sites is supported by the similarity between Cs–Ru/MgO and Ru/MgO with respect to the kinetic parameters derived from the TPD, IER, and TPA experiments. Such promoted sites may originate from the interaction with oxygen vacancies in the alkaline earth support at the interface.

5. For Cs–Ru/MgO, it was possible to predict the TPA peak shape and its position at 380 K based on the rate constants derived from the TPD and IER experiments. The microkinetic analysis showed that the number of promoted sites may depend on temperature. At higher temperatures, more active sites seem to be present which may be ascribed to a two-dimensional fluid–solid equilibrium of the (Cs + O)-coadsorbate layer. Since the unpromoted Ru/Al_2O_3 catalyst was found to be rather inactive for NH_3 synthesis, the presence of the alkali or alkaline earth promoter seems to be essential for Ru-based catalysts.

6. The good agreement between the experimental and calculated results for Cs–Ru/MgO based on a LHHW mechanism indicates that the alkali promotion renders the Ru metal surfaces uniform toward the interaction with N_2.

The initial sticking coefficients and the rate of N_2 desorption derived from the TPD, IER, and TPA experiments for Ru/Al_2O_3, Ru/MgO, and Cs–Ru/MgO are in good agreement with results obtained with Ru single crystal surfaces under ultra-high vacuum conditions. Thus microkinetics served successfully as a tool to bridge the gap between Ru

single crystals in UHV and supported Ru catalysts operating at high pressure.

ACKNOWLEDGMENTS

The authors benefitted from discussions with H. Dietrich, K. Jacobi, R. Schlögl, B. Fastrup, K.-I. Aika, and S. R. Tennison. Some results are obtained with the optimization software developed by W. E. Stewart. O. H. would like to thank J. A. Dumesic and R. Cortright for their help and discussions during his visit at the University of Wisconsin.

APPENDIX: NOTATION

A_i	Preexponential factor	$(\text{kPa} \cdot \text{s})^{-1}$, s^{-1}
E_i	Activation energy	kJ/mol
k_i	Rate constant	$(\text{kPa} \cdot \text{s})^{-1}$, s^{-1}
p	Pressure	Pa
Q	Volumetric flow rate	Nml/min
S	Amount of active sites	μmol/g
R	Gas constant	8.314 J/(K · mol)
r	Rate	μmol/(s · g)
r^{TOF}	Turn-over frequency	s^{-1}
T	Temperature	K
w	Catalyst weight	g
x_{NH_3}	Mole fraction of NH_3	—
β	Heating Rate	K/min

REFERENCES

1. Aika, K.-I., and Tamaru, K., *in* "Ammonia: Catalysis and Manufacture" (A. Nielsen, Ed.), 1st ed., p. 103. Springer-Verlag, Berlin, 1995.
2. Tennison, S. R., *in* "Catalytic Ammonia Synthesis" (J. R. Jennings, Ed.), 1st ed., p. 303. Plenum, New York, 1991.
3. Benner, G. S., Le Blanc, J. R., Lee, J. M., Leftin, H. P., Shires, P. J., and van Dijk, C. P., U.S. Patent 4,568,532, Feb. 4, 1986.
4. Shires, P. J., Cassata, J. R., Mandelik, B. G., and van Dijk, C. P., U.S. Patent 4,479,925, Oct. 30, 1984.
5. Czuppon, T. A., Knez, S. A., III, Schneider, R. V., and Worobets, G., Chem. Engineering, March 1993, presented at the "1993 AICHE Ammonia Safety Symposium, Sept. 1993, Orlando, FL," Vol. 100, No. 3, p. 19, 1993.
6. Rosowski, F., Hinrichsen, O., Muhler, M., and Ertl, G., *Catal. Lett.* **36**, 229 (1996).
7. Danielson, L. R., Dresser, M. J., Donaldson, E. E., and Dickinson, J. T., *Surf. Sci.* **71**, 599 (1978).
8. Matsushima, T., *Surf. Sci.* **197**, L287 (1988).
9. Dietrich, H., Geng, P., Jacobi, K., and Ertl, G., *J. Chem. Phys.* **104**, 375 (1996).
10. Tsai, W., and Weinberg, W. H., *J. Phys. Chem.* **91**, 5302 (1987).
11. Shi, H., Jacobi, K., and Ertl, G., *J. Chem. Phys.* **99**, 9248 (1993).
12. Nielsen, B. O., Luntz, A. C., Holmblad, P. M., and Chorkendorff, I., *Catal. Lett.* **32**, 15 (1995).
13. Rasmussen, P. B., Taylor, P. A., and Chorkendorff, I., *Surf. Sci.* **269/270**, 352 (1992).
14. Shi, H., and Jacobi, K., *Surf. Sci.* **278**, 281 (1992).
15. Anton, A. B., Avery, N. R., Toby, B. H., and Weinberg, W. H., *J. Electron Spectrosc. Relat. Phenom.* **29**, 181 (1983).
16. Feulner, P., and Menzel, D., *Phys. Rev. B* **25**, 4295 (1982).
17. Menzel, D., Pfnür, H., and Feulner, P., *Surf. Sci.* **126**, 374 (1983).
18. Anton, A. B., Avery, N. R., Madey, T. E., and Weinberg, W. H., *J. Chem. Phys.* **85**, 507 (1986).
19. Ertl, G., Lee, S. B., and Weiss, M., *Surf. Sci.* **114**, 515 (1982).
20. Kubota, J., and Aika, K.-I., *J. Phys. Chem.* **98**, 11293 (1994).
21. Rosowski, F., Hornung, A., Hinrichsen, O., Herein, D., Muhler, M., and Ertl, G., *Appl. Catal.*, in press (1996).
22. Knözinger, H., Zhao, Y., Tesche, B., Barth, R., Epstein, R., Gates, B. C., and Scott, J. P., *Faraday Discuss. Chem. Soc.* **72**, 53 (1982).
23. Moggi, P., Predieri, G., Albanesi, G., Papadopulos, S., and Sappa, E., *Appl. Catal.* **53**, L1 (1989).
24. Aika, K., Takano, T., and Murata, S., *J. Catal.* **136**, 126 (1992).
25. Hinrichsen, O., Rosowski, F., Hornung, A., Muhler, M., and Ertl, G., *J. Catal.*, to be published (1996).
26. Dalla Betta, R. A., *J. Catal.* **34**, 57 (1974).
27. Muhler, M., Rosowski, F., and Ertl, G., *Catal. Lett.* **24**, 317 (1994).
28. Fastrup, B., and Nielsen, H. N., *Catal. Lett.* **14**, 233 (1992).
29. Fastrup, B., *Top. Catal.* **1**, 273 (1994).
30. Stewart, W. E., Caracotsios, M., and Sørensen, J. P., "Computational Modeling of Reactive Systems." Butterworth, Stoneham, UK, in press.
31. NAG Fortran Library, Numerical Algorithm Group, 256 Banbury Road, Oxford OX27DE, U.K.
32. Boudart, M., *Chem. Rev.* **95**, 661 (1995).
33. Izumi, Y., Hoshikawa, M., and Aika, K., *Bull. Chem. Soc. Jpn.* **67**, 3191 (1994).
34. Nwalor, J. U., and Goodwin, J. G., Jr., *Top. Catal.* **1**, 285 (1994).
35. Fastrup, B., Muhler, M., Nielsen, H. N., and Nielsen, L. P., *J. Catal.* **142**, 135 (1993).
36. Muhler, M., Nielsen, L. P., and Fastrup, B., *Chem. Phys. Lett.* **181**, 380 (1991).
37. Rosowski, F., Ph.D. thesis, FU Berlin, 1996.
38. Zambelli, T., Trost, J., Wintterlin, J., and Ertl, G., *Phys. Rev. Lett.* **76**, 795 (1996).
39. Kim, K. S., Sinfelt, J. H., Eder, S., Markert, K., and Wandelt, K., *J. Phys. Chem.* **91**, 2337 (1987).
40. Dietrich, H., He, P., Jacobi, K., and Ertl, G., to be published, 1996.
41. Datye, A. K., Logan, A. D., and Long, N. J., *J. Catal.* **109**, 76 (1988).
42. Voskresenskaya, E. N., Roguleva, V. G., and Anshits, A. G., *Catal. Rev.- Sci. Eng.* **37**, 101 (1995).
43. Muhler, M., Rosowski, F., Wild, U., Kowalczyk, Z., and Ertl, G., *J. Phys. Chem.*, to be published (1996).
44. Trost, J., Wintterlin, J., and Ertl, G., *Surf. Sci.* **329**, L583 (1995).
45. Boudart, M., and Djéga-Mariadassou, G., "Kinetics of Heterogeneous Catalytic Reactions." 1st ed. Princeton Univ. Press, Princeton, NJ, 1984.
46. Hinrichsen, O., Rosowski, F., Muhler, M., and Ertl, G., *Chem. Eng. Sci.* **51**, 1683 (1996).